A Fourth-Order Finite-Volume Method with Adaptive Mesh Refinement for Large-Eddy Simulation: Wall-Layer Models

Shumei Yin*, Stephen Guzik†, and Xinfeng Gao‡
Computational Fluid Dynamics and Propulsion Laboratory
Colorado State University, Fort Collins, CO 80523, USA

The wall-layer modeling is investigated in a fourth-order finite-volume method for large eddy simulation (LES) of compressible turbulent flows in simple geometries. Specifically, two zonal-approach models are considered, including a two-layer wall model and a detached-eddy-simulation based method with a Spalart-Allmaras turbulence model. As the initial stage of a LES study for the high-Reynolds number flows in complex geometries, the present investigation, by only considering simple geometries, allows the focus on gaining a thorough understanding of the algorithmic implementation strategies when the high-order discretization, the adaptive mesh refinement, the zonal wall-lay modeling approaches, the accuracy and computational efficiency are taken into consideration. By comparing the results of the wall-layer models, the present study provides some insights into the algorithmic details.

Nomenclature

Accents

$\bar{}$	Filtered quantity
$\breve{}$	Quantity computed in terms of the filtered quantities
$\overleftrightarrow{}$	Tensor
$\vec{}$	Vector
$\tilde{}$	Favre-filtered quantity

Symbols

μ	Molecular viscosity
μ_t	Eddy viscosity
ρ	Density
τ	Molecular fluid stress tensor
e	Total specific energy
f	Body force per unit volume
p	Pressure
q	Molecular heat flux
u	Velocity

I. Introduction

Reynolds-averaged Navier-Stokes (RANS)-based approaches in computational fluid dynamics (CFD) modeling for turbulent flows have plateaued in their ability to resolve the critical technical challenges today.[1]

*Graduate Research Assistant, Email: shumei.yin@colostate.edu, Member AIAA
†Assistant Professor, Email: stephen.guzik@colostate.edu, Member AIAA
‡Associate Professor, Email: xinfeng.gao@colostate.edu, Member AIAA

This is because the RANS approach does not directly resolve the unsteady fluid motions but instead resolves the time-averaged motions. The closure models employed by RANS often invoke some ad hoc hypotheses and assumptions, based on physical intuition or experimental observations. Direct numerical simulation (DNS) can resolve all the fluid scales and motions. However, for engineering applications involving complex geometrical configurations and chemically reacting flows, DNS is prohibitively expensive. Today's computing power can not afford such DNS applications, neither will the computing power over the coming decades. A compromise between RANS and DNS is the large eddy simulation (LES). LES of turbulent flows directly solves the large scales of fluid motions, while implicitly accounting for the small scales by using a subgrid-scale (SGS) model. The growth in the use of LES has been primarily driven by advance in high performance computing, giving us the power needed to start solving CFD problems without time-averaging. This increased level of simulation fidelity in LES has shown great promise and demonstrated clear superiority over the RANS approach for moderately complex geometries. Nevertheless, there are tremendous challenges before LES can realize its potential to expand the current engineering design envelope and eschew industrial stagnation. The challenges and difficulties stem from two aspects: one is directly associated with the numerical algorithms and the other is related to modeling of the unknown terms that are resulted from the filtering process and wall modeling when solid surfaces are the boundaries. Among these issues, this study simply focuses on exploring the zonal-approach wall-layer modeling and gaining insights into the potential challenges when they are implemented in a high-order CFD algorithm with adaptive mesh refinement(AMR).

The LES in the present study is based on explicitly, Favre-filtering Navier-Stokes equations. An explicit filter function is employed to filter the original partial differential equations (PDEs), and this analytical, explicit-filtering process introduces an unresolved term, termed as the sub-analytical-filter-scale (SAS). When the filtered PDEs are discretized on a computational grid, another unresolved term - subgrid-scale (SGS) - is produced. Figure 1 is created to illustrate the difference between SAS and SGS, in addition to a few definitions consistently used in our LES study.

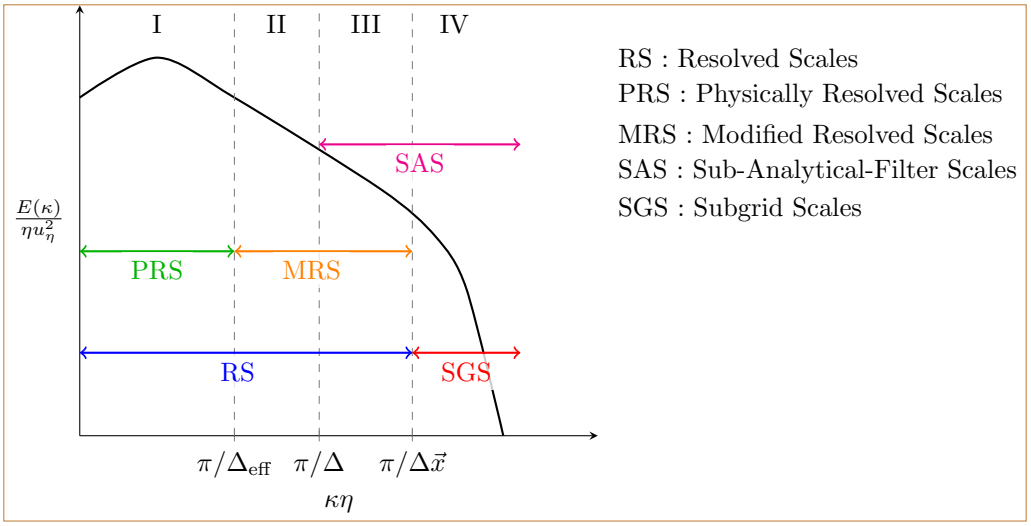

Figure 1: The graphical sketch depicts the scale separation due to an explicitly-filtering, finite-volume scheme, $\kappa_c = \frac{\pi}{\Delta x}$ is the grid cutoff wavenumber.[2]

In the figure, PRS stands for the physically resolved scales and MRS represents the modified resolved scales. The summation of these two terms constitutes RS, that is the resolved scales on the grid. SAS is the sub-analytical-filter-scale and SGS, the sub-grid scales. The effective filter size, Δ_{eff} is a synthetic result from the implicit-filtering (associated with Δx being the grid spacing) and explicit-filtering process (Δ being the explicit filter size). Specifically, when a Smagorinsky SGS model is used, Δ_{eff} can be explicitly evaluated by[3]

$$\Delta_{\text{eff}} = \frac{C_s}{C_A}\Delta\,, \tag{1}$$

where C_s is the SGS Smagorinsky model constant, $C_A \approx 0.2$, and Δ, again, is the analytical filter.

One should distinguish the explicitly-filtering and implicitly-filtering processes. In traditional LES, the computational grid and the discretization method work as implicit filtering, and only introduce SGS turbu-

lence term. The main difference between the implicit and the explicit filtering is that for an implicit filtering process, there is no explicit filter and the filter width is inherently tied to the mesh. This is so-called implicit filter. Thus, as the mesh is refined DNS is recovered and a grid-independent LES solution is not attained. With explicit filtering, one can separate the filtering procedure and filter width from the mesh and therefore grid independent LES solutions are possible. The other advantage of explicit filtering is that it gives a better control of aliasing errors and the appearance of unwanted spurious high-frequency solution contents in the LES solutions.

Furthermore, the implicit-filtered LES should not be confused with the implicit LES (ILES). In an ILES simulation, there is no model employed; rather, the numerical dissipation is used as a closure model. According to Murman et al.,[2] the ILES is at best simulating a flow whose lower Reynolds number cannot be defined. This is clearly illustrated in Fig. (2) and the difference in the resolved wave numbers between the ILES and dynamic LES is shown. Apparently, ILES heavily relied on the discretization schemes and the grid resolution. It will be interesting to see the impact of the high-order finite-volume scheme with AMR in the context of ILES, but this is not the interest of the present work.

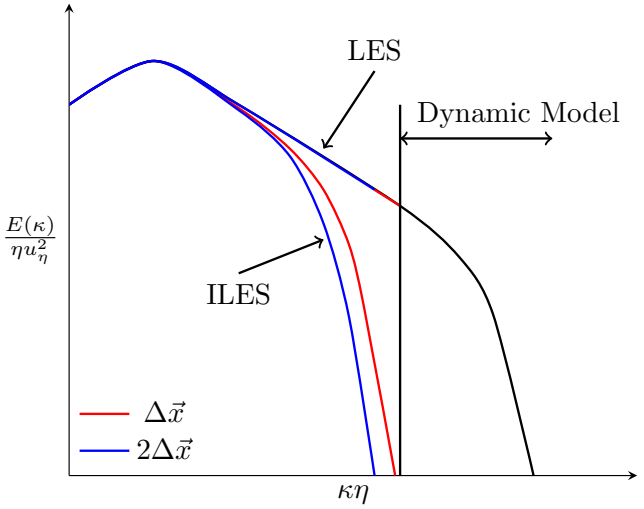

Figure 2: Idealized turbulent spectrum for ILES and dynamic LES simulation. Figure is adapted from Murman.[2]

The paper is structured as follows. Section II describes the mathematical modeling of the LES for compressible flows, including the closure models and wall modeling. Section III presents the computational infrastructure and implementation for the present work. Section IV provides results and discuss the findings. Section V draws conclusions and suggests future follow-up work.

II. Mathematical Modeling of LES for Compressible Flows

II.A. The Explicitly-Filtered Navier-Stokes Equations

LES is based on spatially filtering the instantaneous equations to resolve the contribution of large scales. LES relies on scale separation between energy containing eddies and small scales responsible for its dissipation. The fundamental underlying assumption stems from traditional view of turbulent flows where the bulk of turbulent kinetic energy originates at the large scales. Applying on a random field $\phi(\vec{x},t)$ we get a spatial and temporal filtered random field. The filtered field is defined as:[4]

$$\bar{\phi}(\vec{x},t) = \int_{-\infty}^{\infty}\int_{-\infty}^{\infty} \phi(\vec{\xi},t')G(\vec{x}-\vec{\xi},t-t')dt'd\vec{\xi}\,, \tag{2}$$

where G is the filter convolution kernel function which has the cut off length Δ and cut off time τ_c. In our study, we do not consider the filtering in time domain. And the Favre-filtered variable is defined as:

$$\tilde{\phi}(\vec{x},t) = \frac{\overline{\rho\phi}}{\overline{\rho}}\,, \tag{3}$$

Smaller motions will not be resolved and should be modeled.

The resulting equations governing turbulent flows are spatially filtered mass, momentum, and energy, while the sub-scale effects are modeled. Specifically, the explicitly, low-pass, Favre-filtered form of the

Navier–Stokes equations governing compressible gaseous flows is given by

$$\frac{\partial \bar{\rho}}{\partial t} + \vec{\nabla} \cdot \left(\bar{\rho} \tilde{\vec{u}} \right) = 0 \,, \tag{4}$$

$$\frac{\partial}{\partial t} \left(\bar{\rho} \tilde{\vec{u}} \right) + \vec{\nabla} \cdot \left(\bar{\rho} \tilde{\vec{u}} \tilde{\vec{u}} + \bar{p} \vec{\vec{I}} \right) = \vec{\nabla} \cdot \check{\vec{\vec{\tau}}} + \bar{\rho} \vec{f} + \mathcal{A}_1 + \mathcal{A}_2 \,, \tag{5}$$

$$\frac{\partial}{\partial t} \left(\bar{\rho} \widetilde{e} \right) + \vec{\nabla} \cdot \left[\bar{\rho} \tilde{\vec{u}} \left(\widetilde{e} + \frac{\bar{p}}{\bar{\rho}} \right) \right] = \vec{\nabla} \cdot \left(\check{\vec{\vec{\tau}}} \cdot \tilde{\vec{u}} \right) - \vec{\nabla} \cdot \check{\vec{q}} + \bar{\rho} \vec{f} \cdot \tilde{\vec{u}} + \mathcal{E}_1 + \mathcal{E}_2 + \mathcal{E}_3 + \mathcal{E}_4 \,, \tag{6}$$

where $\bar{\rho}$ is the filtered density, $\tilde{\vec{u}}$ is the Favre-filtered velocity, $\bar{p}$ is the filtered pressure, $\vec{\vec{I}}$ is the identity tensor, $\tilde{e} = |\tilde{\vec{u}}|^2/2 + \tilde{h} - \bar{p}/\bar{\rho}$ is the Favre-filtered total specific energy with $\tilde{h}$ being the enthalpy, and $\vec{f}$ is a body force per unit volume acting on the gaseous mixture. In addition, $\check{\vec{\vec{\tau}}}$ and $\check{\vec{q}}$ are the resolved molecular stress tensor and the resolved molecular heat flux vector, which are computed in terms of the filtered quantities, respectively. The filtered pressure is given by the ideal gas law $\bar{p} = \bar{\rho} R \tilde{T}$, where R is the gas constant and $\tilde{T}$ is the Favre-filtered temperature. The resolved molecular fluid stress tensor is defined as $\check{\vec{\vec{\tau}}} = 2\mu(\check{\vec{\vec{S}}} - \frac{1}{3}\vec{\vec{I}}\,\vec{\nabla} \cdot \tilde{\vec{u}})$ where $\check{\vec{\vec{S}}}$ is the resolved strain rate tensor computed from the Favre-filtered quantities, and μ is fluid molecular viscosity.

In the governing equations, terms $\mathcal{A}_1$, $\mathcal{A}_2$, $\mathcal{E}_1$, and $\mathcal{E}_2$, $\mathcal{E}_3$ and $\mathcal{E}_4$ correspond to sub-analytical-filter-scale (SAS) quantities and require modeling. These terms are given as

$$\mathcal{A}_1 = -\vec{\nabla} \cdot \left[\bar{\rho} \left(\widetilde{\vec{u}\vec{u}} - \tilde{\vec{u}}\tilde{\vec{u}} \right) \right] \,, \tag{7}$$

$$\mathcal{A}_2 = -\vec{\nabla} \cdot \left(\overline{\vec{\vec{\tau}}} - \check{\vec{\vec{\tau}}} \right) \,, \tag{8}$$

$$\mathcal{E}_1 = -\vec{\nabla} \cdot \left(\overline{\rho \vec{u} e} - \bar{\rho} \tilde{\vec{u}} \tilde{e} \right) \,, \tag{9}$$

$$\mathcal{E}_2 = -\vec{\nabla} \cdot \left(\overline{\vec{u} p} - \tilde{\vec{u}} \bar{p} \right) \,, \tag{10}$$

$$\mathcal{E}_3 = \vec{\nabla} \cdot \left(\overline{\vec{\vec{\tau}} \cdot \vec{u}} - \check{\vec{\vec{\tau}}} \cdot \tilde{\vec{u}} \right) \,, \tag{11}$$

$$\mathcal{E}_4 = -\vec{\nabla} \cdot \left(\bar{\vec{q}} - \check{\vec{q}} \right) \,, \tag{12}$$

and they need to be modeled to close the filtered equations.

II.B. Sub-Analytical-Filter-Scale Modeling

To understand and model the unknown terms, Eq. (7) - (12), resulting from the filtering process, we define two general categories based on Fig. (1) in this study. SAS includes regions III and IV. The latter is related to SGS modeling. The former is combined with region II as MRS, which is termed as subfilter scale (SFS) modeling. Next, we will describe the modeling for each category in detail.

II.B.1. Subfilter-Scale Modeling

SFS modeling models the information, as shown in Fig. (1) as MRS, that can be resolved on the grid but is modified due to the fact that the explicitly-defined filter size is greater than the grid spacing, or by the subgrid model. If the filter size decreases, given the grid resolution is fixed, the sum of the SFS and SGS turbulent stresses should decrease. In theory, the SFS stress can be restored through reconstruction by using the filtered solution field. This reconstruction can be performed using the Van Cittert (1913) iterative method via approximate deconvolution procedure. In our study, we are interested in a high-order reconstruction for the SFS modeling terms since the CFD algorithm itself is fourth-order accurate. The reconstruction is a series of successive filtering operations (G) by

$$\phi = \phi_i + (I - G) * \phi_i + (I - G) * ((I - G) * \phi_i) + \dots \,, \tag{13}$$

where I is the identity matrix and "$*$" represents the convolution operator. In our case, the truncation error is $O(\Delta^5)$. However, the details of the SFS modeling is not included in the present study.

II.B.2. Subgrid-Scale Modeling

For SGS modeling, we employ the Smagorinsky model[5] as an starting point and the SGS stress model is given by

$$\sigma_{ij} = -2\mu_t(\check{S}_{ij} - \frac{1}{3}\delta_{ij}\check{S}_{ij})\,, \tag{14}$$

where $\vec{\vec{\sigma}}$ is the SGS stress tensor, μ_t is the SGS viscosity, $\check{S}$ is the resolved strain rate tensor. The SGS viscosity is modeled by

$$\mu_t = \bar{\rho}C_s^2\Delta^2|\tilde{S}|\,, \tag{15}$$

with

$$|\tilde{S}| = (2\check{S}_{ij}\check{S}_{ij})^{1/2}\,. \tag{16}$$

In this model

$$\Delta = (\prod_{d=1}^{D}\Delta x_d)^{1/D}\,,$$

and C_s is a constant, approximately between 0.1 and 0.2 depending on the flow.

The dependence of the Smagorinsky constant on different flows brought about the dynamic Smagorinsky model suggested by Germano et al.[6] where model parameters are calculated from smallest resolved scales on the fly, thus no external information is needed. This method is self-contained and self-consistent. In dynamic model, $C_s^2 = C_d = C_d(x, y, z, t)$. The value of C_d remains the question, but we know that the optimum value is problem dependent and that its value should be reduced near solid walls to reduce the amount of dissipation introduced by the SGS model. However, the dynamic model is left for a follow-up study, since the main goal of the present work is to enable an LES capability in Chord.

Standard gradient-based approximations are used to model The SGS temperature flux (in the form of $\mathcal{E}_1$) and the turbulent diffusion (in the form of $\mathcal{E}_2$) is approximated by the formula suggested by Knight et al.[7] The other two terms arise from the inexact replacement of $\bar{\tau}$ by $\tilde{\tau}$ and $\bar{\vec{\tau}}$ by $\tilde{\vec{\tau}}$ in the derivation of the equations.

II.B.3. Summary of the Models Used in This Work

In the present study, we start with the simple case, assuming and making that the analytical filter is equal to the grid resolution ($\Delta = \Delta\bar{x}$) and the SGS model constant C_s has a small value, meaning that the effective filter corresponds to the analytical filter ($\Delta_{\text{eff}} = \Delta$). In doing so, we are only concerned with the modeling unknown terms, $\mathcal{A}_1$, $\mathcal{A}_2$, $\mathcal{E}_1$, $\mathcal{E}_2$, $\mathcal{E}_3$, and $\mathcal{E}_4$, in the Favre-averaged filtered equations in the context of SGS modeling. That is the region MRS in Fig. (1) disappears. Consequently, Fig. 3 represents this particular case and is reduced from Fig. 1.

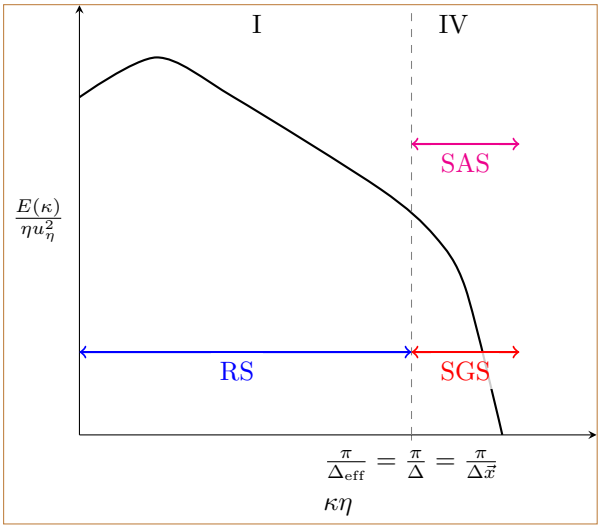

Figure 3: The representative scale separation (reduced from Fig. 1) for the case of interest to the present study.

Specifically, the models are prescribed as follows. In the momentum equation, the subgrid viscous diffusion ($\mathcal{A}_1$) is modeled by the Smagorinsky model as described above, while the $\mathcal{A}_2$ is negligible. In the energy equation, the subgrid energy/heat flux in $\mathcal{E}_1$ is modeled by

$$\mathcal{E}_1 = \vec{\nabla}\cdot\left(\kappa_t\vec{\nabla}\tilde{T}\right) \tag{17}$$

with the turbulent thermal conductivity $\kappa_t = \frac{\mu_t}{Pr_t}C_p$ with μ_t, Pr_t, and C_p being the subgrid viscosity, subgrid Prandtl number, and the specific heat of the fluid. The subgrid turbulent diffusion in $\mathcal{E}_2$ is modeled by

$$\mathcal{E}_2 = \vec{\nabla}\cdot\left[(\check{\vec{\tau}} + \vec{\sigma})\cdot\tilde{\vec{u}}\right]. \tag{18}$$

Furthermore, $\mathcal{E}_3$, and $\mathcal{E}_4$ are considered small and negligible in this study.

II.C. Wall-Layer Modeling

At high Reynolds number, fully-resolved LES is prohibitively expensive due to the small but dynamically important eddies in the near-wall region. Wall model acts as boundary condition for the LES equations. For example, the wall model is used to estimate the wall shear stress (instantaneous) which is typically needed by the boundary conditions to the LES governing equations. A wall model should provide that the mean flow must have logarithmic behavior at the near wall boundary. Two models are investigated: (i) a two-layer model and (ii) the hybrid RANS/LES method with Spalart-Allmaras (SA) model. Details in each model are described next.

II.C.1. A Two-Layer Model

A simple equilibrium wall-model[8] is also known as a two-layer wall shear stress model.

$$\frac{\partial}{\partial y_\perp}\left[(\mu+\mu_t)\frac{\partial \widetilde{u_\parallel}}{\partial y_\perp}\right]=0\ , \tag{19}$$

$$\frac{\partial}{\partial y_\perp}\left[(\mu+\mu_t)\widetilde{u_\parallel}\frac{\partial \widetilde{u_\parallel}}{\partial y_\perp}+c_p\left(\frac{\mu}{Pr}+\frac{\mu_t}{Pr_t}\right)\frac{\partial \widetilde{T}}{\partial y_\perp}\right]=0\ . \tag{20}$$

Eq. (19) and (20) are the conservation equations for streamwise momentum and energy in an equilibrium boundary layer flow. In the equations, $u_\parallel$ is the streamwise (parallel to the wall) velocity and $y_\perp$ is the distance away from wall in its normal direction. Where the eddy-viscosity is given by

$$\mu_t=\kappa\rho y u_\tau\left[1-exp\left(-\frac{y_\perp^+}{A^+}\right)\right]^2\ . \tag{21}$$

Note that $u_\tau\equiv\sqrt{\tau_\omega/\rho}$ is the friction velocity, the velocity scale in a boundary layer with varying mean density with $\tau_w=\mu\frac{d\widetilde{u_\parallel}}{dy}|_{y=0\text{ at the wall}}$. The modeling parameters are $\kappa=0.41$, $Pr_t=0.9$, and $A^+=17$. The "+" superscript represents normalization by viscous wall quantities, such as the friction velocity, e.g. $y^+\equiv\frac{u_\tau y_\perp}{\nu}$, with ν being the kinematic viscosity of the fluid. Nevertheless, it must be noted that the equilibrium model generally works well in attached flows and can reduce computation time by at least one order of magnitude. However, it can not predict separate flows accurately.

For this wall-stress model, the solid surface boundary is assumed to be adiabatic no-slip condition. The upper boundary condition for the wall model is provided by the LES solution at the grids above the wall. Configuration including the grids are shown in Fig. (4). Specifically, a fine grid in the wall normal direction is embedded in the first layer of the LES grid, while keeping the streamline-wise resolution the same. AMR is advantageous for nesting the grid for the inner scales in the LES grid. As illustrated in Fig. (5), mesh is adaptively refined in regions where scales are of interest to resolve. The wall model produces the wall sheer stress and heat flux as the boundary condition for the LES at the solid wall surface.

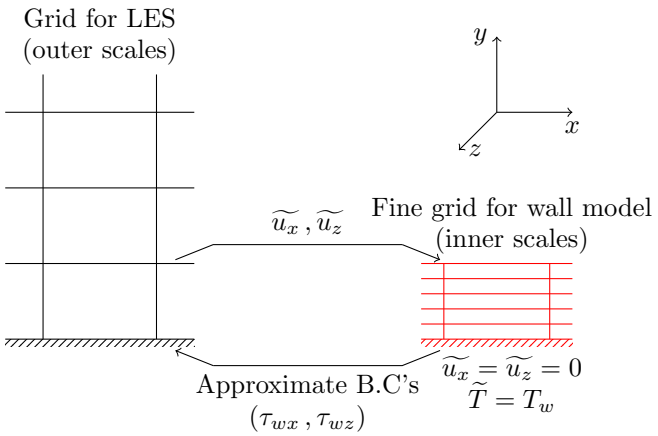

Figure 4: An illustration of the grids for the two-layer wall-stress model.

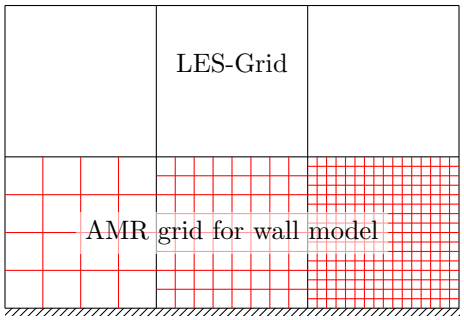

Figure 5: Adaptive mesh refinement in the fine grid for inner scales.

II.C.2. The Spalart-Allmaras Model as A Wall Model

The SA model for the near-wall region compressible equation[9] is used for high turbulence Reynolds number flows, and given by

$$C_{b_1} S \rho \nu_t + \frac{\partial}{\partial y_\perp}\left[\frac{1}{\sigma}\left(\mu + \rho\nu_t\right)\frac{\partial \nu_t}{\partial y_\perp}\right] + \frac{C_{b_2}}{\sigma}\rho\left(\frac{\partial \nu_t}{\partial y_\perp}\right)^2 - C_{w_1} f_w \rho \frac{\nu_t^2}{d^2} = 0\,, \tag{22}$$

where ν_t is the eddy viscosity, S is the magnitude of the vorticity, d the distance to the nearest wall and f_w a non-dimensional function defined by:

$$f_w = g\left(\frac{1 + C_{w_3}^6}{g^6 + C_{w_3}^6}\right)\,,$$
$$g = r + C_{w_2}\left(r^6 - r\right)\,,$$
$$r = \frac{\nu_t}{S k^2 d^2}\,.$$

In the logarithmic layer of a zero pressure gradient boundary layer $f_w \simeq 1$. The model constant are:

$$C_{b_1} = 0.1355\,, \quad C_{b_2} = 0.622\,,$$
$$C_{w_1} = \frac{C_{b_1}}{k^2} + \frac{1 + C_{b_2}}{\sigma}\,,$$
$$\sigma = \frac{2}{3}\,, \quad k = 0.41\,, \quad C_{w_2} = 0.3\,, \quad C_{w_3} = 2\,.$$

In this method, we have experimented two cases. In one test, we use two separate grids (the inner grid and the LES grid) and in the other a single grid (the LES grid) is used.

II.D. Filter Functions

The choice of explicit filter function and filter size in LES equations is critical in terms of the control of discretization errors. For a fourth-order code that is used in this work, the explicit filter width, Δ, should be about at least twice the cell resolution, $\Delta\vec{x}$, that is $\Delta = 2\Delta\vec{x}$.[3] The filter is important in the SFS stress modeling. Note that we chose our analytical filter size the same as our spatial resolution for the reason that the focus of the present study on SGS models. Although it is highly unlikely the MRS disappears as shown in Fig. (3), this highly simplified case allows us to focus on the SGS model implementation. Specifically, in the dynamic Smagorinsky model, the test filter greatly impacts its performance. As a starting point, we use Gaussian function for both explicit and test filters. The test filter width is twice the explicit filter width.

III. Computational Framework

The computational framework for the present work is Chord,[10–15] our in-house CFD code. Chord is a highly parallel, fourth-order accurate, solution-adaptive, finite-volume CFD algorithm on a Cartesian grid. Currently, Chord solves the system of governing equations for transient, compressible, viscous gaseous combusting flow with moderately complex geometries.

Chord has been designed to achieve superior accuracy and parallel performance for simulations of physics where flows exhibit multiscale behavior, such as turbulence, combustion, shock, or plasma. The use of AMR allows for the mesh resolution to change in response to the characteristics of the solution. AMR on a Cartesian grid is logistically simple and efficient. Chord handles complex geometries by mapping a structured grid in physical space to a Cartesian grid in computational space, because finite volume methods employed on Cartesian grids are computationally efficient and additionally benefit from having well-understood properties in terms of solution accuracy. Moreover, finite-volume methods are well suited for problems with discontinuities - the resulting discretization satisfies a discrete form of the divergence theorem, leading to a local conservation property for time-dependent problems.

The high-order finite-volume method can produce solutions to smooth flows much faster than low-order schemes, to the same level of accuracy. For the spatial discretization scheme, a fourth-order center-differencing method is used for computing the face-averaged primitive quantities and the face-averaged gradients, and thus for hyperbolic and elliptic flux evaluation. However, for flows where strong discontinuities or shock waves present, the hyperbolic flux is then evaluated based on the upwind scheme by solving a Riemann problem at each cell face. A piecewise parabolic method limiter is applied to find the left and right face-averaged primitive variable values. The standard fourth-order Runge-Kutta method is employed to evolve the system of governing equations in time. Chord ensures the freestream preservation and enforce stability constraints. Moreover, the high-order methods increase the computation per unit memory which makes better use of modern and upcoming computer architectures. Chord also employs the loop chaining concept for significant improvement in code performance on parallel machines.

IV. Results and Discussion

The wall models are experimented for the turbulent flows over a smooth flat plate aligned parallel to the uniform inflow. Figure 6 illustrates the change in the boundary layer type and thickness over the plate surface. The fluid is air with properties of T = 300K, $\rho = 1.161\,\mathrm{kg/m^3}$, $\mu = 1.846 \times 10^{-5}\,\mathrm{kg/m \cdot s}$ and $Re_L = \rho u_\infty L/\mu = 3.0 \times 10^7$. More frequently, the Reynolds number based on boundary layer thickness δ and wall friction velocity u_τ, $Re_\tau = \rho u_\tau \delta/\mu$, is referred. For convenience, a wall unit is defined $x^+ = x u_\tau/\nu$ for a streamwise location x.

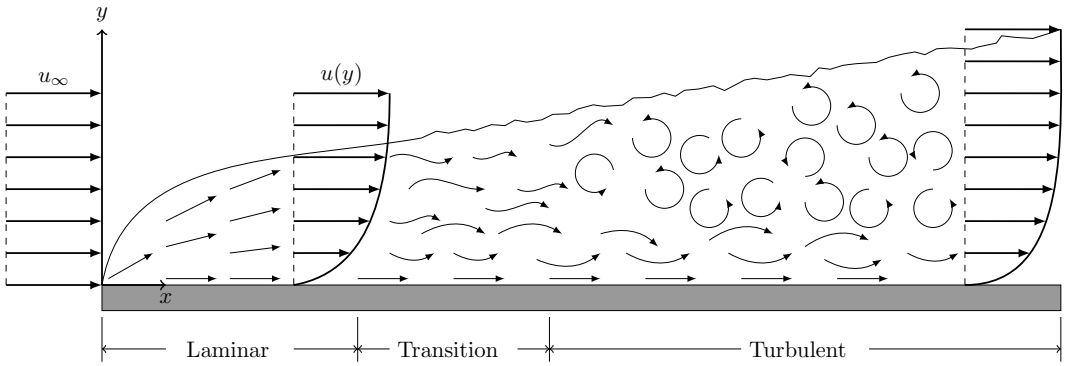

Figure 6: A typical boundary layer development over a flat plate.

Table 1 summarizes the properties of the turbulent boundary layer calculated from this study. Specifically, the quantities, e.g., $\frac{du}{dy}|_{\mathrm{wall}}, \tau_{\mathrm{wall}}, u_\tau$, and $y_1^{+\prime}s$ are reported for the two-layer and SA RANS wall models. From

Table 1: Summary of properties for the turbulent boundary layer over the flat plate.

μ_t Model	h_{wm}	y_1^+	τ_w	u_τ	$\frac{du}{dy}\|_w$
Mixing Length Model	δ	4.20	0.2938	0.5030	15915
	0.3δ	2.57	0.2059	0.4211	11154
	0.3δ	18.45	0.1659	0.3779	8987
	0.1δ	2.39	0.1489	0.3581	8066
SA	0.3δ	2.73	0.2318	0.4467	12257

the Table, it can be seen the difference in the properties obtained from the two models. Importantly, they both provide τ_w at a similar magnitude that is close to the literature data. Further, we examine and compare the velocity profiles for the inner layer. Figure 7 shows the velocity profile sensitivity to y_1^+. Clearly, when the y_1^+ is located in the viscous sublayer region, it reasonably reproduces the law of the wall. The height of the wall model region is also investigated, and as it is shown in Fig. 8 that the near-wall turbulent stress profile can be well predicted with the wall model region of 10% δ. For this simple flat plate case, the inner layer for the wall model can be placed within 10 - 30% of the boundary layer thickness. Moreover, a comparison of $-\bar{\rho}\tilde{u'v'}/\tau_w$ is made by Fig. 9 for two y_1^+'s and the profile behaves better for the small $y_1^+ = 2.6$ than the $y_1^+ = 18.5$. Further, the turbulent Reynolds stress profiles of $-\bar{\rho}\tilde{u'v'}/\tau_w$ versus y/δ are plotted in Fig. 10 for both models. Consistently, we found that SA model predicts a $-\bar{\rho}\tilde{u'v'}/\tau_w$ profile that is not reasonable. Note that the stress profiles show "staircase" behavior which is artifacts from the postprocessing process and will be corrected.

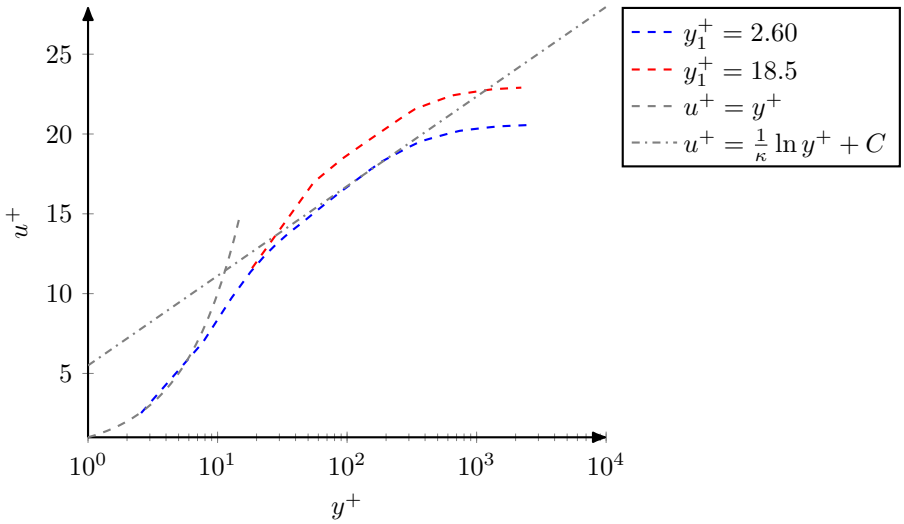

Figure 7: The velocity profile sensitivity to y^+.

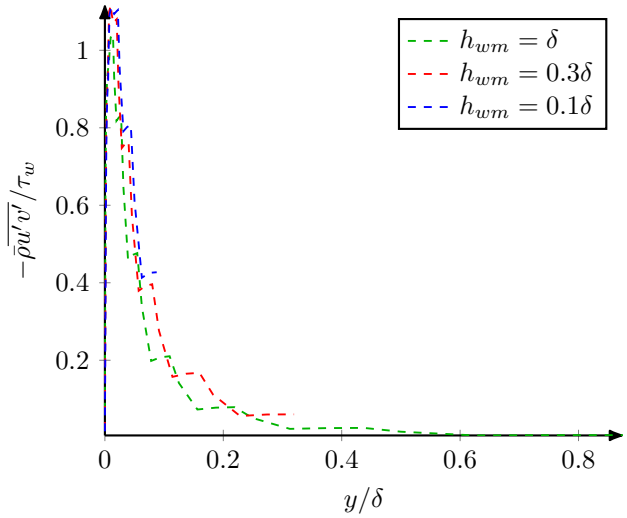

Figure 8: The turbulent stress sensitivity to the inner wall model region height.

As emphasized by Larsson[8] and it is the case in the present study, the wall models can only be expected to function properly if fed accurate information at the top "boundary" from the LES solution, whose accuracy in turn depends on the wall turbulence obtained from the wall models. Essentially, the first y_1^+'s of the LES grid

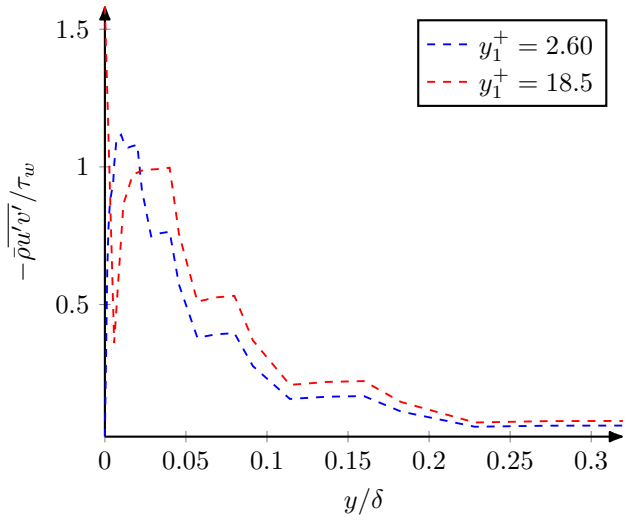

Figure 9: The turbulent stress sensitivity to y_1^+.

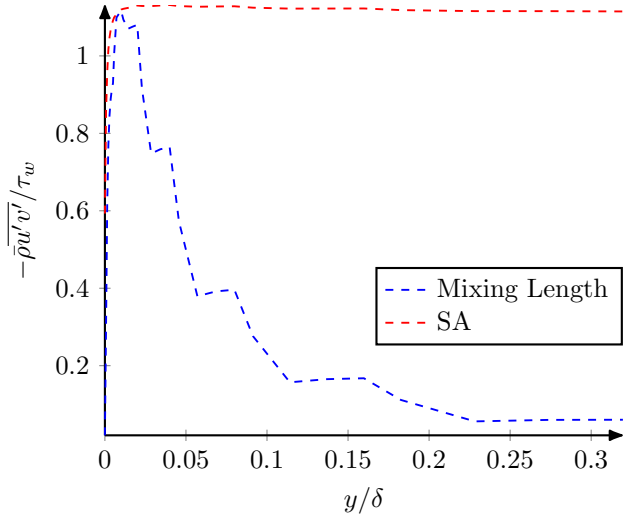

Figure 10: The near wall turbulent stress profiles for the mixing length and SA models.

should sufficiently capture the transition from the viscous sublayer to the outer layer with the appropriate turbulent energy transfer. The first $y^{+\prime}$s are varying at each time step of the calculation. Particularly, for the SA RANS wall model, getting the transition correct is rather challenging.

V. Concluding Remarks and Future Work

Through this study we have explored two wall-layer modeling approaches for the wall-modeled LES simulation of a turbulent flow over a flat plate. The mixing length model appears to be more robust and consistent in producing proper wall properties than the SA RANS model acting as the wall model. There are two possible reasons for the latter - the lack of a precise transition between the SA RANS turbulence and the LES turbulence at the interface, and the lack of the capability of the two-way information transfer between inner and outer layers. Although the second reason may not play an important role in this simple flat plate geometry, it is a more serious factor in complex configurations where the non-equilibrium flows present in the inner layer. Further investigation is required to confirm the sensitivity of the y_1^+ location, the grid spacing in the wall normal direction, and the "actual" y_n (n is the cell index counting from 1 off the wall in the normal direction) in the LES grid that can serve as a good upper boundary for the wall model.

In an immediate follow-up study, we will apply the fourth-order, adaptive finite-volume LES code with the wall-layer modeling methods to a channel flow, including two cases: $Re_\tau = 544$[2] and $Re_\tau = 4000$,[16] for which the literature has detailed information for comparison.

References

[1]Subcommittee, A. S. C. A. C., "The opportunities and challenges of exascale computing," Tech. rep., DOE, 2010.

[2]Murman, S. M., Diosady, L. T., Garai, A., and Ceze, M., "A Space-Time Discontinuous-Galerkin Approach for Separated Flows," AIAA 2016-1059, 54th AIAA Aerospace Sciences Meeting, 2016.

[3]Sagaut, P., *Large Eddy Simulation for Incompressible Flows*, Springer, 3rd ed., 2005.

[4]Garnier, E., Adams, N., and Sagaut, P., *Large Eddy Simulation for Compressible Flows*, Springer, 2009.

[5]Smagorinsky, J., "General circulation experiments with the primitive equation," *Mon. Wea. Rev.*, Vol. 91, 1963, pp. 99–152.

[6]Germano, M., Piomelli, U., Moin, P., and Cabot, W., "A dynamic subgrid-scale eddy viscosity model," *Phys. Fluids A*, Vol. 3, No. 7, 1991, pp. 1760–1765.

[7]Knight, D., Zhou, G., Okong'o, N., and Shukla, V., "Compressible large eddy simulation using unstructured grids," Paper 98-0535, AIAA, January 1998.

[8]Larsson, J. and Kawai, S., "Wall-modeling in large eddy simulation: length scales, grid resolution and accuracy," *Annual Research Briefs*, Center for Turbulence Research, 2010.

[9]Catris, S. and Aupoix, B., "Density corrections for turbulence models," *Aerosp. Sci. Technol.*, Vol. 4, January 2000, pp. 1–11.

[10]Gao, X., Guzik, S. M. J., and Colella, P., "Fourth Order Boundary Treatment for Viscous Fluxes on Cartesian Grid Finite-Volume Methods," AIAA 2014-1277, 52nd AIAA Aerospace Sciences Meeting, 2014.

[11]Gao, X. and Guzik, S. M. J., "A Fourth-Order Scheme for the Compressible Navier-Stokes Equations," AIAA 2015-0298, 53rd AIAA Aerospace Sciences Meeting, 2015.

[12]Guzik, S. M., Gao, X., Owen, L. D., McCorquodale, P., and Colella, P., "A Freestream-Preserving Fourth-Order Finite-Volume Method in Mapped Coordinates with Adaptive-Mesh Refinement," *Comput. Fluids*, Vol. 123, 2015, pp. 202–217.

[13]Gao, X., Owen, L. D., and Guzik, S. M. J., "A Parallel Adaptive Numerical Method with Generalized Curvilinear Coordinate Transformation for Compressible Navier-Stokes Equations," *Int. J. Numer. Meth. Fluids*, Vol. 82, 2016, pp. 664–688.

[14]Gao, X., Owen, L. D., and Guzik, S. M., "A High-Order Finite-Volume Method for Combustion," AIAA 2016-1808, 54th AIAA Aerospace Sciences Meeting, 2016.

[15]Gao, X., Wang, Y., Overton, N., May, I., and Tu, X., "Data Assimilated Computational Fluid Dynamics Algorithm for Combustion," *54th AIAA Aerospace Sciences Meeting*, No. AIAA 2016-1810, AIAA SciTech Forum, 2016, `https://doi.org/10.2514/6.2016-1810`.

[16]Cabot, W. and Moin, P., "Approximate Wall Boundary Conditions in the Large-Eddy Simulation of High Reynolds Number Flow," *Flow, Turbulence and Combustion*, Vol. 63, 1999.